Aerodynamic Modelling for a Morphing Rudder

M. A. Castillo-Acero[1], C. Cuerno-Rejado[2] and M. A. Gómez-Tierno[2]

[1]Aernnova, Av. Manoteras, 20, 5th, 28050, Madrid. Spain. miguelangel.castillo@aernnova.com

[2] Escuela Técnica Superior Ingenieros Aeronáuticos, UPM, Pza. C. Cisneros, 3, 28040, Madrid, Spain

Abstract

The appearance of new materials and smaller and more capable actuators enable the morphing controlled deformation of the aerodynamic shape of wing like type of structures. This contribution presents the applied aerodynamics studies of a morphing rudder for a commercial transport aircraft. The conventional rudder aerodynamics is CFD modeled and the results correlated to certification loads report. The morphing rudder CFD model predicts better aerodynamics efficiency in relation to the conventional one. This conclusion is the first step for future commercial aircraft Vertical Tail Plane weight reductions with morphing rudder implementation.

Keywords: Morphing, Aerodynamic, CFD, Vertical Stabilizer, Rudder, Turbulence modeling.

NOMENCLATURE

2D: Two dimensions
3D: Three dimensions
C: Courant number
c_D: Aerodynamic resistance coefficient
CD_{kw}: Distance, on k-w model
c_L: Aerodynamic lift coefficient
c_m: Aerodynamic moment coefficient
C_o: Dimension of the original cell
CFD: Computational fluid dynamics
D: Characteristic dimension of the first fluid cell model in contact with wall
DNS: Direct Numerical Simulation
EASA: European Airworthiness Safety Agency
FAA: Federal Aviation Administration
Fi: Mix Functions
IATA: International Air Transport Association
k: Kinetic energy
LES: Large Eddy Simulation
M: Mach number
NACA: National Advisory Committee for Aeronautics
Nl: Number of layers
Nr: Refinement level,
NS: Navier Stokes equations
OF: Open Foam
$p, \tilde{p}$: Pressure
P_k: Turbulence generation
PISO: Pressure Implicit Split Operator,
R: Reduction of the moment arm
RANS: Reynolds-averaged Navier-Stokes
Re: Reynolds number
S: Invariant measure of the strain rate
SMA: Shape Memory Alloys
SST: Shear Stress Transport
t: Time
$\tilde{T}_{ij}^{(v)}$: Viscosity tensor components
UAV: Unmanned Aerial Vehicle
U_∞: Velocity non perturbed fluid domain
u, $(\tilde{u}_i)$: velocity
VTP: Vertical Tail Plane
ω: Specific dissipation
x, $(\tilde{x}_i)$: distance
y_+: Non-dimensional distance to fluid wall
$\alpha, \beta, \gamma, \sigma$: Constants
ϵ: Expansion ratio
ε: Turbulent dissipation
$\tilde{\rho}$: Fluid density
ρ_{FLT}: Size relation between the most exterior layer and the one in contact with the wall
v: Kinematic viscosity
v_t: Turbulent kinematic viscosity

I. INTRODUCTION

The aeronautics commercial industry is characterised for its continuous improvements and the introduction of aircraft models more fuel and cost efficient,

increasing the quality standards, technical integrity and compliance, if possible in advance, with the airworthiness requirements. One of the effects is the continuous decrease in the cost per passenger (per ton-m in the case of freight operations) and kilometre. According to IATA statistics, this average improvement yields a yearly figure of 2%. In the other hand, the different air traffic prognosis sources, predict an average over 4% increment per year. This means that, currently, the whole commercial aeronautics chain is under pressure to optimize the operations to fill this gap, [1], in particular aircraft manufacturers and their supply chains, including their technology extended enterprises. The fact that fuel consumption reduction decreases the CO_2 emissions, together with the fuel costs rising and representing higher share of the direct operating costs, and the long time foreseen future scarcity of fossil sources, makes the fuel consumption the star on current optimization and search for efficiency efforts. This study includes the works to develop a new VTP morphed rudder, for a defined as objective commercial transport aircraft type, to increase the vertical empennage aerodynamics efficiency and so reduce its structural weight.

This study includes several aerodynamic models in order to develop a new vertical tail plane morphed rudder. The targeted new rudder with enhanced aerodynamics efficiency corresponds to a commercial high by-pass ratio turbofan aircraft, podded engines under low wing, and 90 passengers' payload. The literature provides examples on the utilization of morphing for the benefit of aerodynamic improvements, a good summary can be found in reference [2]. The development of several families of smart materials enables their application on airfoils, controlling their deformation for different purposes. Among others and to present the diversity of materials solutions it can be mentioned micro- reinforced- composites [3], shape memory alloys, SMA, nitinol-based that modifies the natural frequency of composite structures [4], shape memory polymers for wing skins, [5], bi-stable laminated composites [6]. The onset delay of the laminar to turbulent thanks to smart bumps is also a promising field for first application of these new materials, like the ones in reference [7]. All these studies concentrate on wings rather than empennage stabilizers and most of them aim for an application to the design of innovative, UAV, as referenced in [2].

The airfoil of the vertical empennage considered in this work is NACA 64A010. The morphing considered on this study is theoretical. Two smooth curves, at extraback and intrados, are considered. They connect the fixed part ending corner points with a continuously curved rudder, rear portion of it flat. See Fig. 1.

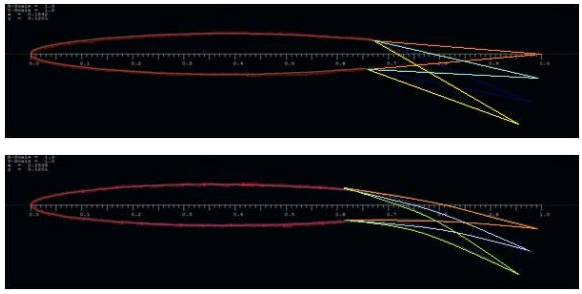

Figure 1 NACA64010 and rudder deflection without and with morphing

It is left for further analysis which curves families create the optimum and more efficient effect.

In practical terms, this curves can be based on retractable trailing edge panels with a selective deformable material, as in references [8], [9], [10] or [11] just to cite some examples, to provide two continuous surfaces (both sides of the airfoil) together with the addition of an articulated ribs mechanism as in reference [12].

II. METHODOLOGY

The VTP and the rudder of typical transport commercial airplanes are sized by means of three load cases, more critical than the rest: "rudder kick", "lateral gust" and "one engine out" load cases.

The engine out condition is critical at take off, M<0.3 and requires total rudder deflection, it is to say 30º for the reference airplane in this work. This is the critical load case than usually sizes most of the rudders and the biggest proportion of the vertical stabilizer fixed part.

In this study, numerical aerodynamic models based on CFD are developed, aiming to provide solutions for the 3D geometries of the VTP. The selected CFD has been Open Foam because it is under continuous development by many different research groups worldwide, reference [13]. Open Foam is based on C++ libraries that can be modified and customized to fit the complexity of each problem and it also allows changes in the fundamental physical formulation. The Open Foam models can account for air compressibility effects together with the viscosity effects on the turbulence and the boundary layer analysis in relation to the more simplistic panels' methods, i.e. XFOIL [14], or vortex lattice methods, i.e. Tornado [15]. Computational limitations based on lack of convergence for 3D and 30 º deflections have been suffered in this study. This is a very demanding computing scenario due to the adverse pressure gradients, flow separation, and the complexity of the turbulence model.

The Open Foam code allows selecting the solver, steady or unsteady types, the turbulence model and the boundary conditions that depend on the geometry and, also, on the solver and turbulent model selected. The best processing selections for the accuracy of the calculations concluded in this study are:

- transient unsteady solver Pimple Foam, based on PISO, and semi implicit methods, for the low velocity, below M=0,3 so uncompressible regime. The Pimple Foam better fits for long time intervals and high deflection aerodynamic case
- and Sonic Foam for the other case, high velocity, compressible regime.

Open Foam also allows controlling the time intervals. The time intervals have been introduced depending on the Courant number. The non dimensional Courant number provides a relation between the solving time and the residency time of a fluid particle in a given volume. In the present case this volume is the cells one and the Courant number must be lower than one in the entire domain to assure adequate convergence.

$$C = \frac{\Delta t}{\frac{\Delta x}{u}} = \frac{u\Delta t}{\Delta x} < 1 \qquad (1)$$

Moreover, due to the transient methodology selected, the solving time must be big enough to allow that a fluid particle runs the whole domain. This brings the question about whether the domain volume is big enough. For the problem under this study, 6 times the characteristic, chord length, has been considered.

Nowadays there are different ways to solve turbulent flows, through Navier- Stokes equations or direct simulation. The selection of a RANS model for this study, and not a LES or a DNS one, is because it better fits the resolution scale to the requirements. Figure 2 shows the different scales for different turbulent model techniques, [16].

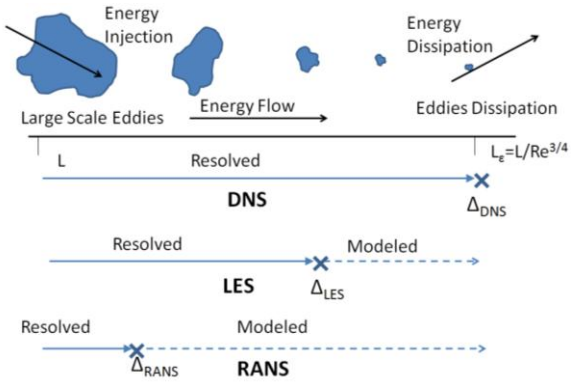

Figure 2 Turbulent Models and related scales

In order to properly model the turbulence with RANS in Open Foam, the fundamentals behind Navier- Stokes equations have to be clearly understood.

$$\rho\left(\frac{\partial \tilde{u}_i}{\partial t}+\tilde{u}_j\frac{\partial \tilde{u}_i}{\partial x_j}\right)=-\frac{\partial \tilde{p}}{\partial x_i}+\frac{\partial \tilde{T}_{ij}^{(v)}}{\partial x_j} \quad (2)$$

$$\left(\frac{\partial \tilde{\rho}}{\partial t}+\tilde{u}_j\frac{\partial \tilde{\rho}}{\partial x_j}\right)+\tilde{\rho}\frac{\partial \tilde{u}_j}{\partial x_j}=0 \quad (3)$$

$$\tilde{T}_{ij}^{(v)}=2\mu\left(\tilde{s}_{ij}-\frac{1}{3}\tilde{s}_{kk}\delta_{ij}\right) \quad (4)$$

$$\tilde{s}_{ij}=\frac{1}{2}\left(\frac{\partial \tilde{u}_i}{\partial x_j}+\frac{\partial \tilde{u}_j}{\partial x_i}\right) \quad (5)$$

All variables that describe instantaneous flow present a tilde, these are the fluid density ($\tilde{\rho}$), velocity ($\tilde{u}_i$), pressure ($\tilde{p}$) and tensor components of viscous effects ($\tilde{T}_{ij}^{(v)}$). These variables are all dependent on time and space. The first equation as stated above corresponds to the momentum equation, Newton's second law for fluids. The second is the equation of continuity. The tensors of viscous stresses are the latest.

If incompressible flow requirements are introduced, then equations are simplified considerably.

$$\left(\frac{\partial \tilde{u}_i}{\partial t}+\tilde{u}_j\frac{\partial \tilde{u}_i}{\partial x_j}\right)=-\frac{1}{\tilde{\rho}}\frac{\partial \tilde{p}}{\partial x_i}+\vartheta\frac{\partial^2 \tilde{u}_i}{\partial x_j^2};\ \vartheta\equiv\frac{\mu}{\rho} \quad (6)$$

$$\frac{\partial \tilde{u}_j}{\partial x_j}=0 \quad (7)$$

$$\tilde{T}_{ij}^{(v)}=2\mu\tilde{s}_{ij} \quad (8)$$

Decomposing the turbulent variables into two components, the mean and the fluctuating:

$$\tilde{u}_i=U_i+u_i \quad (9)$$

$$\tilde{p}=P+p \quad (10)$$

$$\tilde{T}_{ij}^{(v)}=T_{ij}^{(v)}+\tau_{ij}^{(v)} \quad (11)$$

The Navier- Stokes equations become:

$$\rho\left[\frac{\partial(U_i+u_i)}{\partial t}+(U_j+u_j)\frac{\partial(U_i+u_i)}{\partial x_j}\right]=-\frac{\partial(P+p)}{\partial x_i}+\frac{\partial\left(T_{ij}^{(v)}+\tau_{ij}^{(v)}\right)}{\partial x_j} \quad (12)$$

$$\rho\left[\frac{\partial U_i}{\partial t}+U_j\frac{\partial U_i}{\partial x_j}\right]=-\frac{\partial P}{\partial x_i}+\frac{\partial}{\partial x_j}\left(T_{ij}^{(v)}-\rho\langle u_iu_j\rangle\right) \quad (13)$$

Thus the terms known as Reynolds stresses appear, with the same structure and dimensions that the terms of viscous stresses without representing an actual stress, but rather a mathematical modeling. These terms provide new variables to the problem, without additional relations or equations to solve them. It could be tried to model as if they really were a stress, trying to empirically obtain constitutive relations, however these relationships are typical of a fluid, while turbulence is associated with the flow and change as the conditions do. This makes it impossible to obtain valid constitutive relations to model turbulence and forced to turn to other methods, this is the "closure problem" of the Navier -Stokes equations: a priori it is not possible to close the problem due to lack of equations. From here different types of modeling can be defined.

This study is also based on considering Boussinesq Hypothesis, as in references [17] or [18] for similar problems, and the already mentioned [16], that establishes a linear relation between the Reynolds stresses and the average strains in a fluid, and can be written as follows, being μ_t the Eddy viscosity:

$$-\rho\langle u_iu_j\rangle=2\mu_tS_{ij}-\frac{2}{3}\rho k\delta_{ij} \quad (14)$$

Where k is the average kinetic energy and S is the mean deformation:

$$k=\frac{1}{2}(\langle u_1u_1\rangle+\langle u_2u_2\rangle+\langle u_3u_3\rangle) \quad (15)$$

$$S_{ij}=\frac{1}{2}\left[\frac{\partial U_i}{\partial x_j}+\frac{\partial U_j}{\partial x_i}\right]-\frac{1}{3}\frac{\partial U_k}{\partial x_k}\delta_{ij} \quad (16)$$

Therefore the problem is simplified to model the turbulent viscosity. There are different approaches: algebraically or zero equations approach, one equation and two equations. The first one does not provide valid results but it results good to obtain initial values for others more complex approaches. The one equation approach solves the kinetic energy transport in relation to the turbulent viscosity with additional coefficients and equations, like Prandtl model or Spatart-Almaras, used for some sensitivity checking, see complete description on reference [18].

Finally two equations models are the most interesting for this case of study. They are widely used in industry, also actively studied in many universities and constantly improved by these. There are several documents about them like references [19], [20] the already cited [18] and [21] from the same author. These models include two extra transport equations to represent the properties of the turbulent flow. The selection of these two equations models is due to the good description of the flow history, as the diffusion and the convection of the turbulent energy effects. The first variable computed is *k*, the turbulent energy density, the choice of the second depends on the scale of turbulence, spatial or temporal; the turbulence dissipation, ε, and the specific turbulent dissipation, ω, have been considered. The turbulence dissipation is the rate at which turbulence kinetic energy transform to thermal energy. The specific turbulent dissipation it is also known as the mean frequency of turbulence.

$$\omega = \frac{\varepsilon}{k\beta^*} \qquad (17)$$

The $k-\varepsilon$ model has been proven useful for modeling flows with wall boundary conditions, internal flows, and small pressure gradients. It has been checked that the accuracy is greatly reduced when large adverse pressure gradients appear. The traditional $k-\omega$ model provides good results in the above conditions and behaves much better to adverse pressure gradients, however predicts the separation of the boundary layer before it should be, and it also requires good resolution near the wall, which increases the computational resources. It has been selected, a SST $k-\omega$ turbulent model that combines $k-\omega$ close to the solid wall, boundary layer or inner region, and $k-\varepsilon$ in the outer region. In order to couple the solutions in these two regions, a blending function with the addition of a formulation for the turbulent viscosity to account for turbulent shear stresses has been used. Thus, the use of a $k-\omega$ formulation in the boundary layer makes the model directly usable to the viscous sublayer, this enables its utilization as a low Reynolds model. The formulation of the SST also changes to a $k-\varepsilon$ behavior in the free stream avoiding the typical problem of $k-\omega$ original, which is very sensitive to initial conditions to turbulent stream input. This decision has proved to be the best choice to analyze this problem, which presents big adverse pressure gradients and flow separation.

The final equations that govern this model, that can also be found in reference [22] are summarized as follows:

$$\frac{\partial k}{\partial t} + U_j\frac{\partial k}{\partial x_j} = P_k - \beta^* k\omega + \frac{\partial}{\partial x_j}\left[(v+\sigma_k v_t)\frac{\partial k}{\partial x_j}\right] \qquad (18)$$

$$\frac{\partial \omega}{\partial t} + U_j\frac{\partial \omega}{\partial x_j} = \alpha S^2 - \beta\omega^2 + \frac{\partial}{\partial x_j}\left[(v+\sigma_\omega v_t)\frac{\partial \omega}{\partial x_j}\right] + 2(1-F_1)\sigma_{\omega 2}\frac{1}{\omega}\frac{\partial k}{\partial x_i}\frac{\partial \omega}{\partial x_i} \qquad (19)$$

$$F_1 = \tanh\left\{\left\{\min\left[\max\left(\frac{\sqrt{k}}{\beta^*\omega y};\frac{500v}{y^2\omega}\right);\frac{4\rho\sigma_{\omega 2}k}{CD_{k\omega}y^2}\right]\right\}^4\right\} \qquad (20)$$

$$CD_{k\omega} = \max\left(2\rho\sigma_{\omega 2}\frac{1}{\omega}\frac{\partial k}{\partial x_i}\frac{\partial \omega}{\partial x_i};10^{-10}\right) \qquad (21)$$

The first equation represent the turbulent kinetic energy, *k,* transport and the second the specific dissipation. F_1 is the mixing or coupling function. CD_{kw} is the distance to the nearest wall. F_1 is zero far away from the wall and takes unit value within the boundary layer, creating change between the $k-\varepsilon$ model and the $k-\omega$.

The turbulent kinematic viscosity v_t is expressed in function of another mix function F_2.

$$v_T = \frac{k}{\max\,(\omega, SF_2)} \qquad (22)$$

$$F_2 = \tanh\left[\left[\max\left(\frac{2\sqrt{k}}{\beta^*\omega y};\frac{500v}{y^2\omega}\right)\right]^2\right] \qquad (23)$$

The turbulence generation in the backwater areas is limited:

$$P_k = \min\left(\tau_{ij}\frac{\partial U_i}{\partial x_j};10\beta^* k\omega\right) \qquad (24)$$

The constants are derived by interpolation with F_1 and F_2 the ones that come from models $k-\varepsilon$ and $k-\omega$

$$\phi = \phi_1 F + \phi_2(1-F) \qquad (25)$$

The constants considered are:

$$\sigma_{\omega 1} = 0.5;\ \sigma_{\omega 2} = 0.856$$

$$\beta_1 = {}^{3}/_{40};\ \beta_2 = 0.0828;\ \beta^* = 0{,}09$$

$$\alpha_1 = {}^{5}/_{9};\ \alpha_2 = 0.44$$

$$\sigma_{k1} = 0.85;\ \sigma_{k2} = 1$$

One of the key characteristics of the CFD model is the wall treatment. The refinement of the CFD models is based on the non-dimensional distance to the fluid wall y_+. This parameter is defined as the ratio between the distance multiplied by the friction velocity and the kinematic viscosity

$$y_+ = u_* y/v < 2 \qquad (26)$$

The Slichting boundary layer Theory, reference [23], has also been used to obtain the dimension of the first cell in contact with the wall dimension, y_+. The average y_+ value has to be around 30 and not bigger than 200, for this study set of boundary conditions, fluidic wall and turbulent models. Although in some cases to reach enough precision without using wall functions for the turbulence, it is required a value of 2, [21], [24]. The application of the Slichting boundary layer theory, available in reference [25], provides that for the subsonic scenario, $U_\infty = 60\ m/s$, sea level, dry air assumption, $\rho = 1{,}225 \frac{Kg}{m^3}$, $v = 1{,}82e-05\ \frac{kg}{m\,s}$, $y_+ = 30$, Reynolds number $Re = 4{,}0e+06$, first cell in contact with the wall dimension: D=20 mm. Based on this value the derivation of the number of layers, Nl, of the CFD model is preformed, so that the value obtained for D in the equation below is the same as obtained before:

$$D = \frac{C_o * \rho_{FLT}}{2^{Nr} \epsilon^{Nl}} \qquad (27)$$

The number of cells obtained for the 3D CFD model exceeds 20 million, two order of magnitude higher than the 2D models.

As the fluid in the models is the air flow, the external forces caused by gravity are neglected. To complete the data entered to Open Foam models, the air is modeled as a perfect gas, hypothesis valid enough for the purposes of the present approach.

This study uses the approach summarized before, for the development of CFD Open Foam models duplicated for the two configurations, the conventional rudder, with an unrealistic closed gap between the fix part and the rudder, and the new morphed one, also closed gap. It has been selected the close gap modeling for the conventional rudder to subtract this effect out of the study and simply consider the effect of the non conventional curved rudder in comparison with the conventional flat one.

The calculations efforts are concentrated on two aerodynamic load cases:

- a low subsonic regime, M < 0.3 and high rudder deflection, 30 º,
- a high subsonic regime, M= 0.8 and a moderate, 10º, rudder deflection.

The models considered, with no slippage, are the following ones:

- 2D CFD, low velocity, for the 30º deflected rudder case, aerodynamic profile at 1/3 vertical stabilizer height
- 2D CFD, high velocity, for 10º rudder deflection, and same reference profile
- 3D CFD, high velocity, for the 10º rudder deflection

This study has not been able to perform a full 3D CFD model that provides results for the low velocity and 30º rudder deflection cases. In order to mitigate this situation, the assumption of a linear approach is performed. The results for CFD models of high velocity and 10º in 3D and 2D provide linear ratios. Then these ratios are applied into the 2D low velocity and 30º deflection case to achieve values for the full 3D low velocity and 30º rudder deflection case.

Figure 3 shows the 3D CFD airfoil, with the 30º rudder deflection. Figure 4 shows the

includes the entire fluidic domain including the VTP mesh.

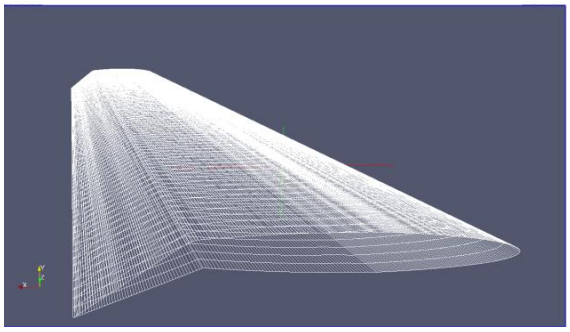

Figure 3 VTP Open Foam 3D mesh.

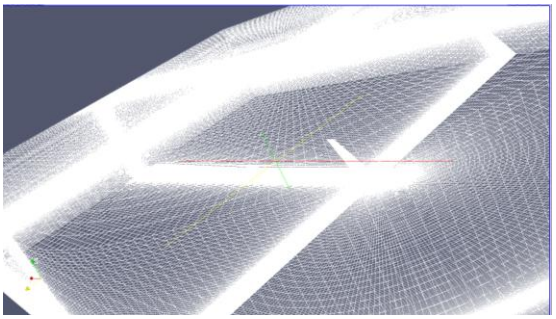

Figure 4 Complete 3D Open Foam mesh.

III. RESULTS AND DISCUSSION

The 2D CFD results, at sea level, aircraft take-off velocity for engine out case U_∞=60 m/s and 30 º conventional rudder deflections are summarized in next paragraphs. The airfoil corresponds to 1/3 height of the VTP. Figure 5 shows the pressure distribution, and Fig. 6 the velocity, at t= 0.17 s moment, when convergence has been achieved. The turbulent wake appears on the velocity graph.

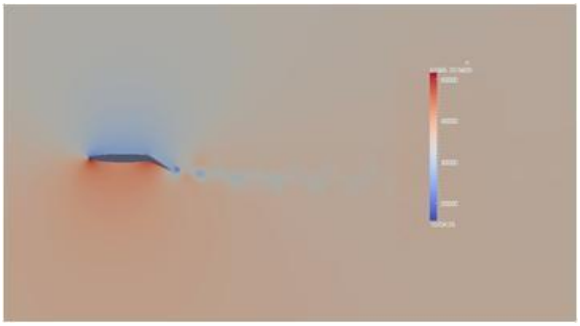

Figure 5 Pressure distribution U_∞=60 m/s, 30º conventional, t=0.17 s

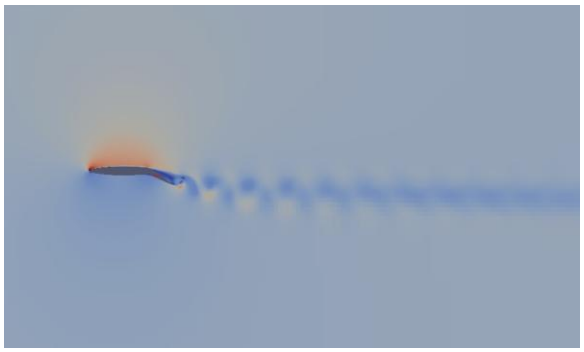

Figure 6 Velocity dist., U_∞=60 m/s, 30 º conventional, t=0.17 s

Figure 7 depicts the evolution of the aerodynamic coefficients with time, between t=0 and t=0.17 s. The wake oscillations and the values stabilization at final time t=0.17 s appear quite clear.

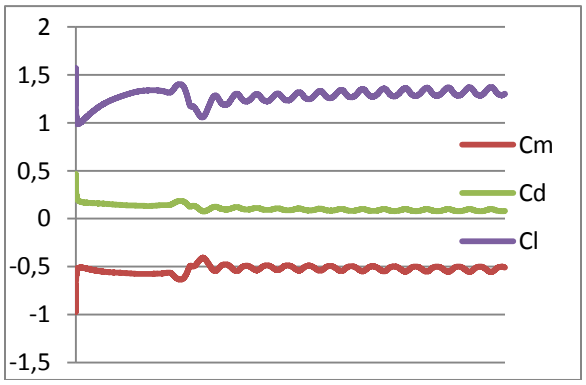

Figure 7 Aerodynamic coefficients time evolution up to t=0.17s, U_∞=60 m/s, 30 º

The turbulent mixing length is checked to be smaller than the scale of variation of the mean pressure and velocity quantities. This validates, partially, the Boussinesq hypothesis, [26].

Figure 8 includes the relative pressure distribution along the airfoil. Note the pressure peak at intrados at 65% of the non-dimensional chord just at rudder chord portion start.

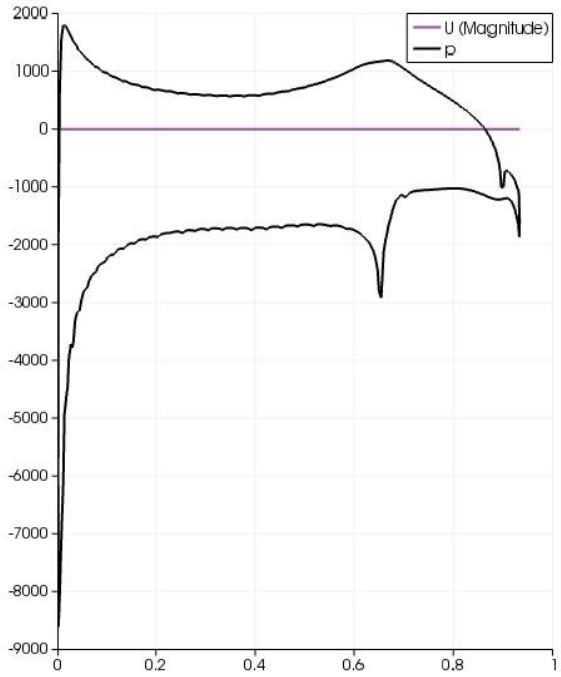

Figure 8 Relative pressure distribution, profile 1/3 height, t=0.17s, U_∞=60 m/s, 30 º

The second aerodynamic load case is 2D Open Foam modeled with the following conditions: 10º conventional rudder, typical cruise velocity of U_∞ =240 m/s, altitude 8000 m, air density 0.45 kg/m^{3}and external air pressure of 35000 Pa. The results are summarized below corresponding to an achieved stabilization at t=0.1 s after 1 hour processing with 8 PCUs.

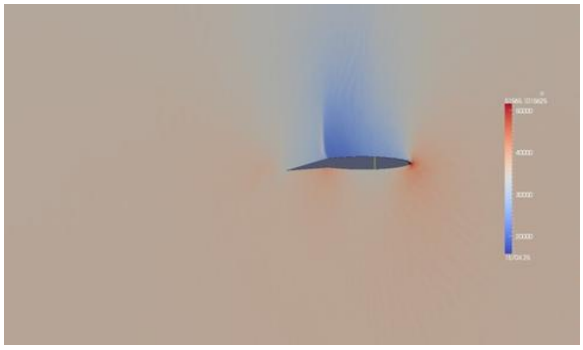

Figure 9 Pressure distribution U_∞=240 m/s, 10º conventional, t=0.1 s

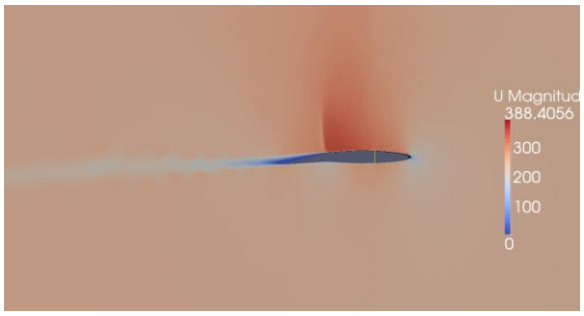

Figure 10 Velocity distribution, U_∞=240 m/s, 10º conventional, t=0.1 s

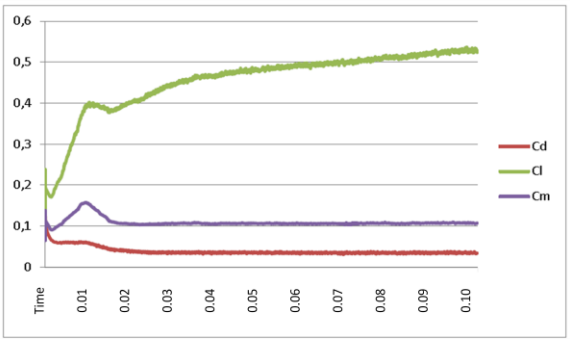

Figure 11 Aerodynamic coefficients time evolution U_∞=240 m/s, 10º conventional

Note that starting at t=0.025 s, the moment and drag coefficients are stable. The lift coefficient increases 20% until final stabilization at t=0.1 s.

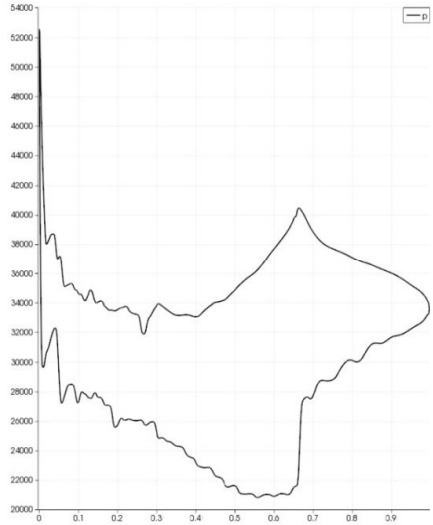

Figure 12 Absolute pressure distribution, profile at 1/3 VTP height span, t=0.1s, U_∞=240 m/s, 10º conventional rudder deflection.

The third case corresponds with a full 3D CFD model, 10º conventional rudder, typical cruise velocity of U_∞ =240 m/s, altitude 8000 m, air density 0.45 kg/m^3 and external air pressure of 35000 Pa. The results are summarized below with a processing time of t=0.025 s. This is the considered time limit due to computation constraints and the fact that with this processing time, as obtained in the case before, the changes on the drag and moment coefficients values are negligible. The computer processing time required is 375 hours with 64 PCUs.

The pressure and velocity distributions can be obtained chordwise at any height station, in particular, for the root and the tip sections and then check the time evolution of them. For simplification purposes, the velocity and pressure distribution at section 1/3 VTP height has been selected in order to compare with previously obtained results.

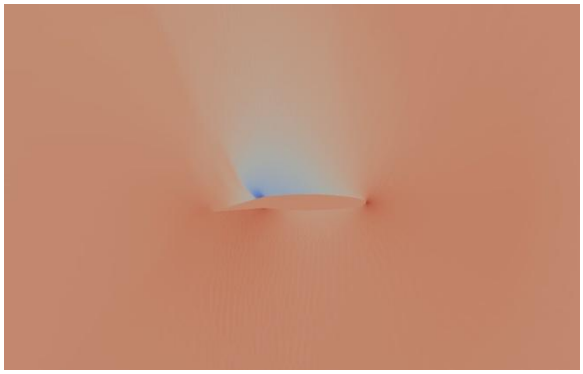

Figure 13 Pressure distribution U_∞=240 m/s, 10º conventional, t=0.1 s. Full 3D

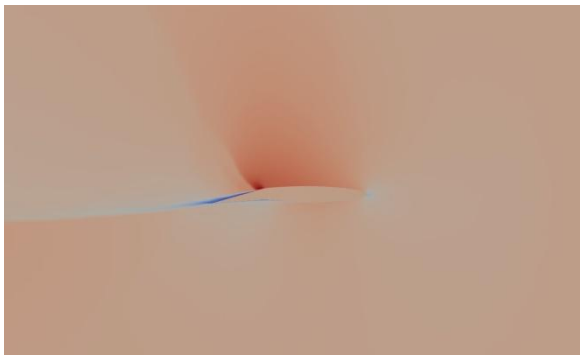

Figure 14 Velocity distribution U_∞=240 m/s, 10º conventional, t=0.1 s. Full 3D

Figure 15 shows the extraback pressure distribution on the empennage and Fig. 16 the intrados for the same case

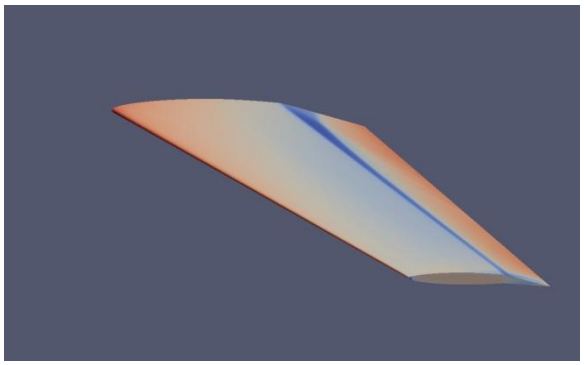

Figure 15 Pressure distribution extraback U_∞=240 m/s, 10º conventional, t=0.025 s. Full 3D

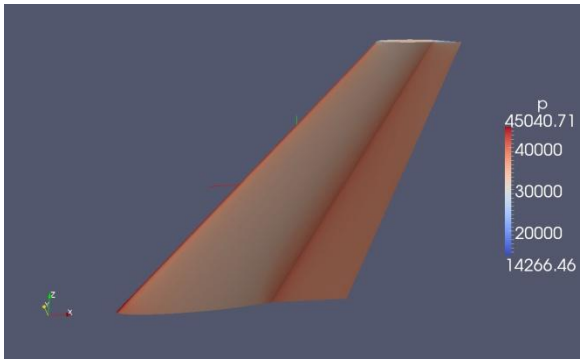

Figure 16 Pressure distribution intrados U_∞=240 m/s, 10º conventional, t=0.025 s. Full 3D

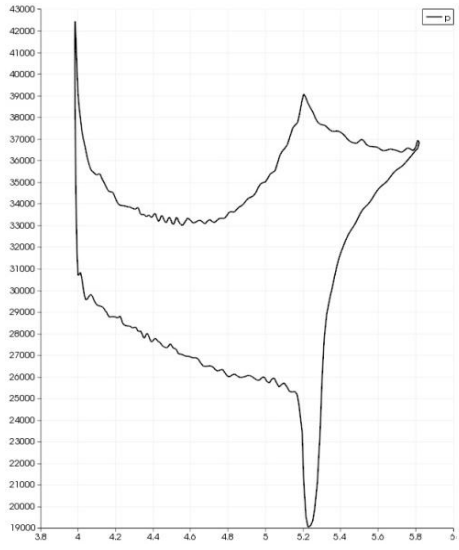

Figure 17 Absolute pressure distribution, profile 1/3 height, t=0.1s, U_∞=240 m/s, 10º conventional rudder, 3D

Comparing previous 2D and 3D CFD Open Foam models, high speed and 10º rudder, result on:

$$c_L 2Dof / c_L 3Dof = 1.4 \qquad (28)$$

$$c_D 2Dof / c_D 3Dof = 0.9 \qquad (29)$$

The reasons for these differences are:

- the swept angle that reduces the aerodynamic efficiency due to the incidence angle .
- the effect of the tip without fairings on the stabilizer and low slenderness that implies a wash out effect.

In order to validate the 3D corrections a Tornado model has been developed, reference [15]. Tornado can account for 3D effects and has been documented to study similar problems, as in [27], [28], [29] and [30]. Therefore with Tornado the full 3D vertical empennage can be analyzed, low velocity 60 m/s, and also a 2D control case, 1/3 span airfoil and same conditions. Tornado enables compressibility effects correction according to the theory of Prandtl-Glauert, although at these velocities corresponding to a Mach number of less than 0.3 effects of compressible air are negligible. For this case study, as before, the aircraft is flying without slippage and the rudder is deflected 30 degrees. After Tornado study aerodynamic coefficients correction factors between 3D and 2D are concluded, as follows:

$$c_L 2Dt / c_L 3Dt = 2.0 \qquad (30)$$

$$c_D 2Dt / c_D 3Dt = 0.9 \qquad (31)$$

The Tornado lift coefficient correction is even bigger than previous 2D- 3D Open Foam comparison. This is due to the selection of the 1/3 span airfoil that is not as accurate as if it is considered the result of averaging Tornado 3D results, closer to 40% span, Fig. 18. This accounts for an additional 1.2 factor due to the bigger chord considered in the Tornado 2D study.

When multiplied by the Open Foam correction of 1.4, yields the factor of 2 that the Tornado approach is predicting.

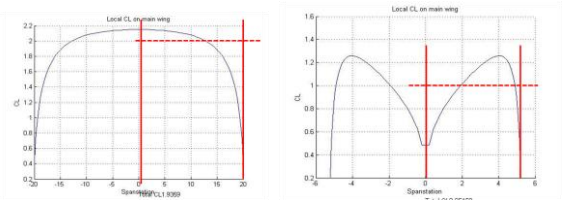

Figure 18 Tornado 2D and 3D results

Finally, the aerodynamic loads from corrected with the Open Foam CFD approach are compared with certification VTP loads for EASA/ FAA take off velocities with engine out scenario (60 m/s). The aerodynamic loads from corrected Open Foam CFD models are integrated at the more forward vertical stabilizer point that is the reference point for certification loads, to obtain OF_c3D values at first column in Table 1 below. The certification VTP loads for EASA/ FAA take off velocities with engine out scenario (60 m/s) are included in the second column. Then the errors between these two set of values are included in column 3.

	OF_c3D	$Certif.$	eOF_c3D
$Fy\ (N)$	35533	31257	13.7 %
$Mx\ (Nmm)$	78473	73857	6.2 %
$Mz\ (Nmm)$	39157	33635	16.4 %

Table 1 Loads comparison: aerodynamic CFD correlations and certification report for engine out take-off condition, Limit Loads

The Open Foam models with 3D adjustments corrections provide bigger loads than the ones reported for certification. The reason for these differences is the well known effect, [31], that closed gap configurations have on a more aerodynamic efficiency than the open ones. The lift forces are higher, and drag ones lower when the gap between fix and movable part is closed. In the case of the lift for a 33% hinge balanced chord blunt edge rudder, a 1.10 factor is expected between closed gap lift configurations and opened one.

Subtracting "gap" effect, an averaged 3% difference for the lateral rudder force, between the results of these studies and the certification loads for the engine out control case can be concluded, which is considered that validates this approach.

The 2D CFD Open Foam, U_∞=60 m/s and 30º morphed rudder provides the results included in Figs 19, 20, 21 and 22. The comparison between Fig. 20 and Fig. 6 shows similar results for velocities distribution.

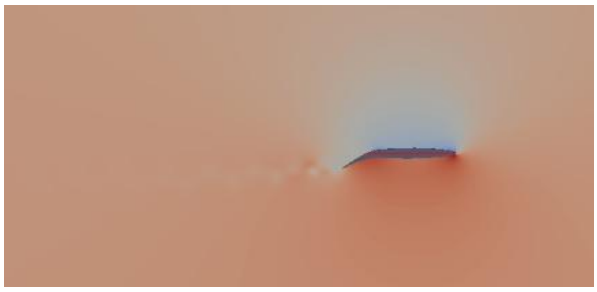

Figure 19 Pressure distribution U_∞=60 m/s, 30º morphed rudder, t=0.24 s

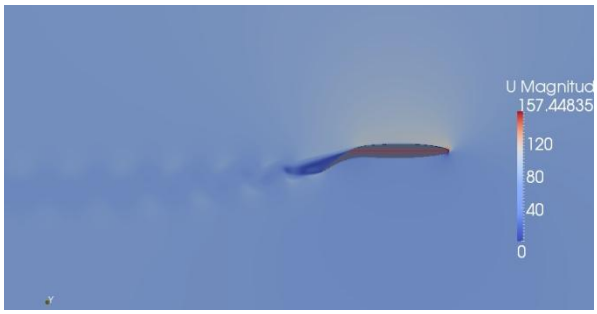

Figure 20 Velocity distribution U_∞=60 m/s, 30º morphed rudder, t=0.24 s

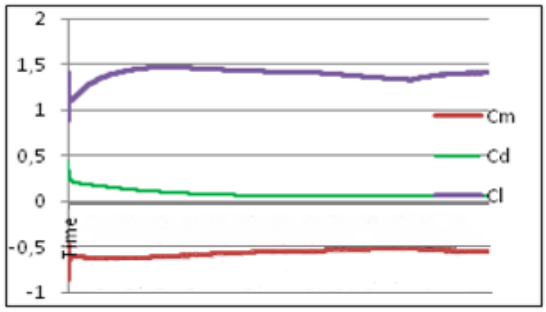

Figure 21 Aerodynamic coefficients time evolution up to t=0.2s, U_∞=60 m/s, 30 º

When comparing Fig. 21 with Fig. 7, it is evident the different behaviour of the coefficients between morphed and conventional rudder. There are no great oscillations due to the different behaviour of the wake that is much smoother.

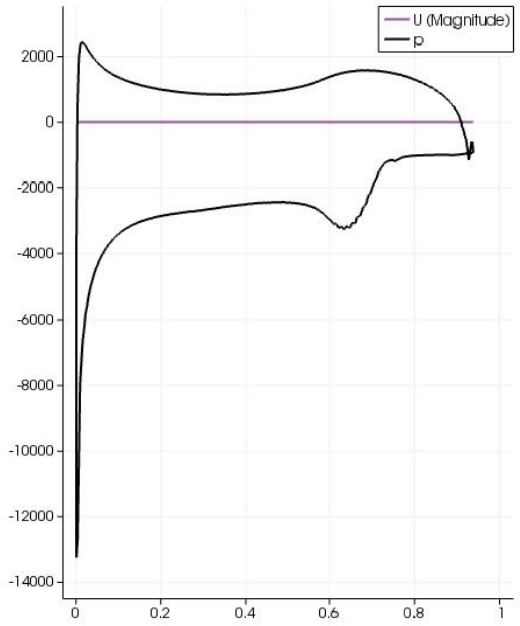

Figure 22 Chordwise vertical tail plane pressure (Pa), 2D CFD Open Foam, 60 m/s, 30 º morphed rudder.

Table 2 includes a comparative of the aerodynamic coefficients values obtained for the study control case, considering the mean value of the periodic oscillations when the convergence time is achieved.

	c_L	c_D	c_m
Closed Gap Conventional Rudder	1,33	0,10	-0,53
Morphing Rudder	1,41	0,06	-0,55
Ratio	1,06	0,60	1,03

Table 2 Aerodynamic Coefficients for Traditional and Morphing Rudder, control case

The results of the comparison with the conventional rudder yields a 6% improvement in vertical stabilizer lateral force and a 40% reduction of the overall drag force for the one engine out case. Therefore a more aerodynamic efficient morphed rudder can be concluded and then translated into weight savings. Moreover, after subtracting the lift increment from the torsion moment

coefficient comparison, a reduction of the moment arm, R is obtained as follows:

$$\frac{c_m}{c_L} = R \qquad (32)$$

	R
Conventional Rudder	0,40
Morphing Rudder	0,39
Ratio	1,025

Table 3 Torsion moment arm effect, control case

The arm of torsion moment is reduced 2.5 %. This means that for the same lateral force in the control surface, the sustained torsion by the fixed part is reduced by this factor that could be also translated into weight savings.

IV. CONCLUSIONS

As a result of comparing pressure distribution for morphing configuration, Fig. 22, in relation to conventional, Fig. 7, several conclusions can be highlighted:

- Peak pressure enhancements at extraback and intrados
- Extraback flat area average pressure improved when morphed
- Intrados pressure enhancement at control surface area
- Rudder extraback pressure redistribution, peak to blunt, and higher average values

These results, point out that the efficiency of the VTP is improved with the morphed rudder. The lateral force developed by the morphed rudder is 16% higher than the conventional one. Therefore, further studies on designing feasible morphing rudder architectures are considered adequate for future consideration.

V. REFERENCES

[1] ATAG, "A sustainable flightpath to reducing emissions. UNFCCC Climate Talks, Doha," no. Nov. p.6, 2012.

[2] S. Barbarino, O. Bilgen, R. M. Ajaj, M. I. Friswell, and D. J. Inman, "A Review of Morphing Aircraft," *J. Intell. Mater. Syst. Struct.*, vol. 22, no. 9, pp. 823–877, Aug. 2011.

[3] L. Butt, S. Day, J. Weaver, C. Sossi, A. Wolek, V. Tech, W. Mason, and D. Inman, "Wing morphing design utilizing macro fiber composite smart materials," in *SAWE Paper No 3515-S*, 2010, vol. 33, no. 3515, pp. 1–61.

[4] M. A. Hariri, "Control Structures Using SMA Wires Piezoelectric Patches" PhD Thesis, RMIT University, 2009.

[5] S. Jee, "Development of Morphing Aircraft Structures using SMP," Air Force Institute of Technology Wright-Patterson Air Force Base, Ohio, 2010.

[6] C. G. Diaconu, P. M. Weaver, and F. Mattioni, "Concepts for morphing airfoil sections using bi-stable laminated composite structures," *Thin-Walled Struct.*, vol. 46, no. 6, pp. 689–701, Jun. 2008.

[7] E. Stanewsky, "Adaptive wing and flow control technology," *Prog. Aerosp. Sci.*, vol. 37, no. 7, pp. 583–667, 2001.

[8] J. Simpson, L. Anguita-Delgado, B. Nilsson, V. Vincenzo, and G. Kawiecki, "Review of the European Research Project 'Active Aeroelastic Aircraft Structures (3As),'" *Eur. Conf. Aerosp. Sci.*, p. 9, 2004.

[9] E. A. Bubert, "Highly Extensible Skin for a Variable Wing-Span Morphing Aircraft Utilizing Pneumatic Artificial Muscle," Master of Science Thesis University of Maryland, 2009.

[10] Robert D Vocke, C. S. Kothera, B. K. S. Woods, E. A. Bubert, and N. M. Wereley, "One Dimensional Morphing Structures for Advanced Aircraft," *Air Force Res. Lab. through a Phase I STTR (contract no FA9550-06-C-0132), also Phase I SBIR Proj. from NASA Langley Res. Cent. NNX09CF06P)*, p. 27, 2007.

[11] C. Thill, J. Etches, I. Bond, K. Potter, and P. Weaver, "Morphing skins," *Aeronaut. J.*, vol. March, no. 3216, pp. 1–23, 2008.

[12] R. Pecora, F. Amoroso, and M. Magnifico, "Design and Experimental Validation of a Morphing Wing Flap Device," in *6th ECCOMAS Conference on Smart Structures and Materials,* 2013, no. June, pp. 24–26.

[13] O. F. Foundation, "Open FOAM." http://www.openfoam.org/ 2014

[14] M. Drela and H. Youngren, "XFOIL." http://www.xflr5.com/xflr5.htm. MIT, 2014.

[15] Tornado: KTH, Royal Ins. Technology in Stockholm, University of Linköping, University of Bristol, UK. http:// www.redhammer.se/tornado. 2014.

[16] J. Sodja, "Turbulence models in CFD," Working paper, University of Ljubljana Faculty, Mathematics & Physics, 2007.

[17] M. Montagnac, "Numerical Simulations Around Wing Control Surfaces," ICAS 2004, 24th International Congress of the Aeronautical Sciences, p. 12. 2004.

[18] J. Bredberg, "On Two-equation Eddy-Viscosity Models," in *Internal Report 01/8 Department of Thermo and Fluid Dynamics Chalmers U. Of Technology. Goteborg, Sweden*, 2001, p. 46.

[19] D. C. Wilcox, *Turbulence Modeling for CFD*. Ed. DCW Industries. La Cañada. CA. USA. 1994, p. 477.

[20] D. C. Wilcox, "Simulation of Transition with a Two-Equation Turbulence Model," *AIAA J.*, vol. 32, no. 2, pp. 247–255, 1994.

[21] J. Bredberg, "On the Wall Boundary Condition for Turbulence Models," in *Internal Report 01/8 Department of Thermo and Fluid Dynamics Chalmers U. Of Technology. Goteborg, Sweden*, 2000, p. 25.

[22] F. R. Menter, M. Kuntz, and R. Langtry, "Ten Years of Industrial Experience with the SST Turbulence Model," *Turbul. Heat Mass Transf. 4*, vol. 4, pp. 625–632, 2003.

[23] H. Schlichting, *Boundary -layer Theory*, 7th Ed. New York. McGraw-Hill. 1979

[24] S. B. Pope, "Chapter 7: Wall Flows," in *Turbulent Flows*, Cambridge University Press, 2000.

[25] Several,"http://www.cfd-online.com/." Accessed: Nov-2013.

[26] F. G. Schmitt, "About Boussinesq's turbulent viscosity hypothesis: historical remarks and a direct evaluation of its validity," *Comptes Rendus Mécanique*, vol. 335, no. 9–10, pp. 617–627, Sep. 2007.

[27] D. A. Neal, D. J. Inman, and C. Woolsey, "Design , Development , and Analysis of a Morphing Aircraft Model for Wind Tunnel Experimentation," Master of Science Virginia Polytechnic Institute and State University in, 2006.

[28] R. Vos, Z. Gurdal, and M. Abdalla, "Mechanism for Warp-Controlled Twist of a Morphing Wing," *J. Aircr.*, vol. 47, no. 2, pp. 450–457, Mar. 2010.

[29] B. Obradovic and K. Subbarao, "Modeling of Flight Dynamics of Morphing Wing Aircraft," *J. Aircr.*, vol. 48, no. 2, pp. 391–402, Mar. 2011.

[30] L. Arrison, "2002-2003 AE / ME Morphing Wing Design," Generic Paper. 2003.

[31] D J Lyons and P. L. Bisgood, "An Analysis of the Lift Slope of Aerofoils of Small Aspect Ratio, Including Fins, with Design Charts for Aerofoils and Control Surfaces," *Aeronaut. Res. Counc. Memo.*, vol. no. 1, p. 26, 1945.